A Global Study of Transition Zone Thickness. S53A-1300

B. Tauzin, E. Debayle and G. Wittlinger

Ecole et Observatoire des Sciences de la Terre, UMR 7516 Université Louis Pasteur and CNRS, Strasbourg, France
benoit.tauzin@eost.u-strasbg.fr

INTRODUCTION

We present global observations of P-to-s conversions at the 410 and 660 km-depth discontinuities of the mantle transition zone (MTZ). We have collected several thousand three-component broad-band seismograms and we compare results for three major tectonic provinces that we have defined for the transition zone : "plume", "normal mantle" and "subduction zones". Taking into account the likely error measurements, we investigate in details whether there are significant differences between stations belonging to the different provinces, consistent with olivine phase transformations. The quality of the Pds measurements is checked by comparing our results with global and regional tomographic models. Results strongly rely on the choices made in the data selection (the frequency range of analysis, the selected range of back-azimuth at the station and the geographical distribution of stations).

Our differential travel-times tP660s-tP410s suggest a thicker MTZ for "subduction zones" compared to "normal mantle". However , within our frequency band of analysis, the "plume region" does not seem to differ significantly from the normal mantle.

DATA SELECTION & PROCESSING

We use the data collected at the broad-band stations of the Geoscope, IRIS-USGS, IRIS-IDA, PACIFIC21, Global Telemetered, Canadian and China global arrays (figure 4) for earthquakes of magnitude (mostly Mw) higher than 6.0 and with epicentral distances between 40° and 90°. After instrument response egalisation, signal-to-noise ratio selection, band-pass (0.1-0.04 Hz) filtering of the data, we use an iterative time-domain deconvolution in the P Sv Sh frame to perform P-to-s receiver function PRFs [1]).

The 26350 PRFs finally selected are stacked within bins of 0.5 distance, aligned on the direct P arrival and plotted in figure 1. Clear P-to-s conversions at the 410 and 660 km depth discontinuities appear respectively at about 45s and 65s after direct P arrival.

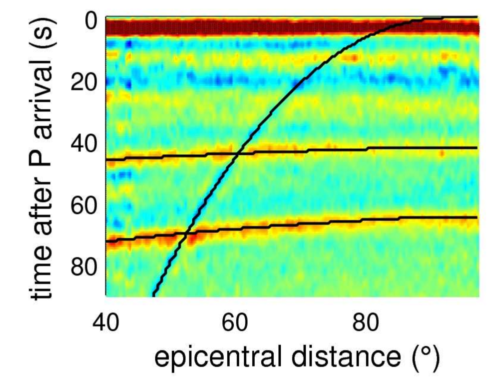

Figure 1. Averaging (stacking) large numbers of RF enhances signals of converted phases which may be too small to be observed on individual receiver functions.

At each station, we built a slant stack (figure 2) of the selected RFs. Move out corrections are performed for a reference epicentral distance of 65°. A stacked time migrated RF (figure 3) is obtained by extracting the amplitude on the theoretcal time-slowness curve (in black in figure 2) computed in IASP91 ([2]).

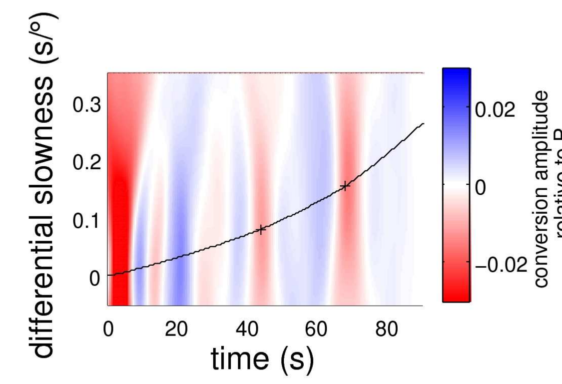

Figure 2.

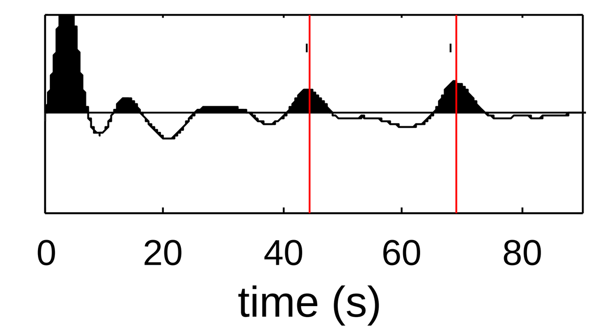

Figure 3.

Global results

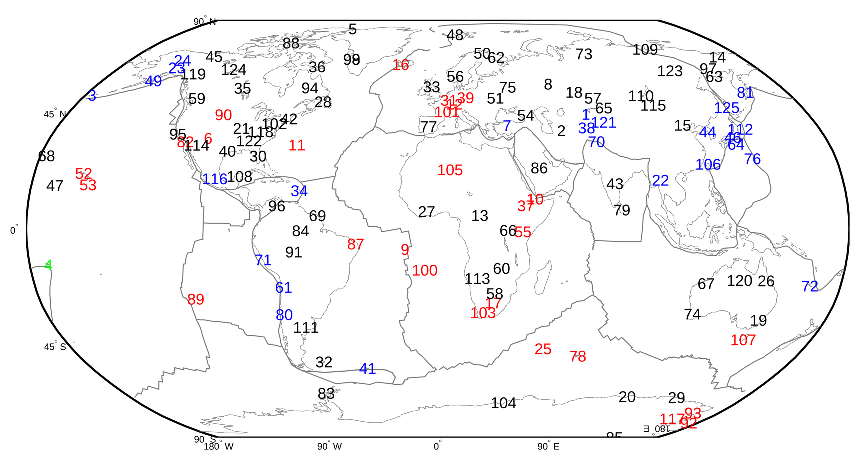

1 AAK	21 CCM	41 HOPE	61 LVC	81 PET	101 SSB	121 WUS
2 ABKT	22 CHTO	42 HRV	62 LVZ	82 PFO	102 SSPA	122 WVT
3 ADK	23 COL	43 HYB	63 MA2	83 PMSA	103 SUR	123 YAK
4 AFI	24 COLA	44 INCN	64 MAJO	84 PTGA	104 SYO	124 YKW3
5 ALE	25 CRZF	45 INK	65 MAKZ	85 QSPA	105 TAM	125 YSS
6 ANMO	26 CTAO	46 INU	66 MBAR	86 RAYN	106 TATO	
7 ANTO	27 DBIC	47 JOHN	67 MBWA	87 RCBR	107 TAU	
8 ARU	28 DRLN	48 KBS	68 MIDW	88 RES	108 TEIG	
9 ASCN	29 DRV	49 KDAK	69 MPG	89 RPN	109 TIXI	
10 ATD	30 DWPF	50 KEV	70 NIL	90 RSSD	110 TLY	
11 BBSR	31 ECH	51 KIEV	71 NNA	91 SAML	111 TRQA	
12 BFO	32 EFI	52 KIP	72 NOUC	92 SBA	112 TSK	
13 BGCA	33 ESK	53 KIP	73 NRIL	93 SBA	113 TSUM	
14 BILL	34 FDF	54 KIV	74 NWAO	94 SCHQ	114 TUC	
15 BJI	35 FFC	55 KMBO	75 OBN	95 SCZ	115 ULN	
16 BORG	36 FRB	56 KONO	76 OGS	96 SDV	116 UNM	
17 BOSA	37 FURI	57 KURK	77 PAB	97 SEY	117 VNDA	
18 BRVK	38 GAR	58 LBTB	78 PAF	98 SFJ	118 WCI	
19 CAN	39 GRFO	59 LLLB	79 PALK	99 SFJD	119 WHY	
20 CASY	40 HKT	60 LSZ	80 PEL	100 SHEL	120 WRAB	

Figure 4 and table 1 Map and name of stations used in this study. Each station is associated with one of the 3 tectonic provinces ("plume", "normal mantle" and "subduction zones") that we have defined for the MTZ. Stations close to subductions are indicated in blue; stations close to hotspots are shown in red; other stations are assumed to belong to the "normal mantle" region; one station belonging to both "plume" and "subduction" regions is shown in green;

tP410s-tP residuals relative to IASP91.

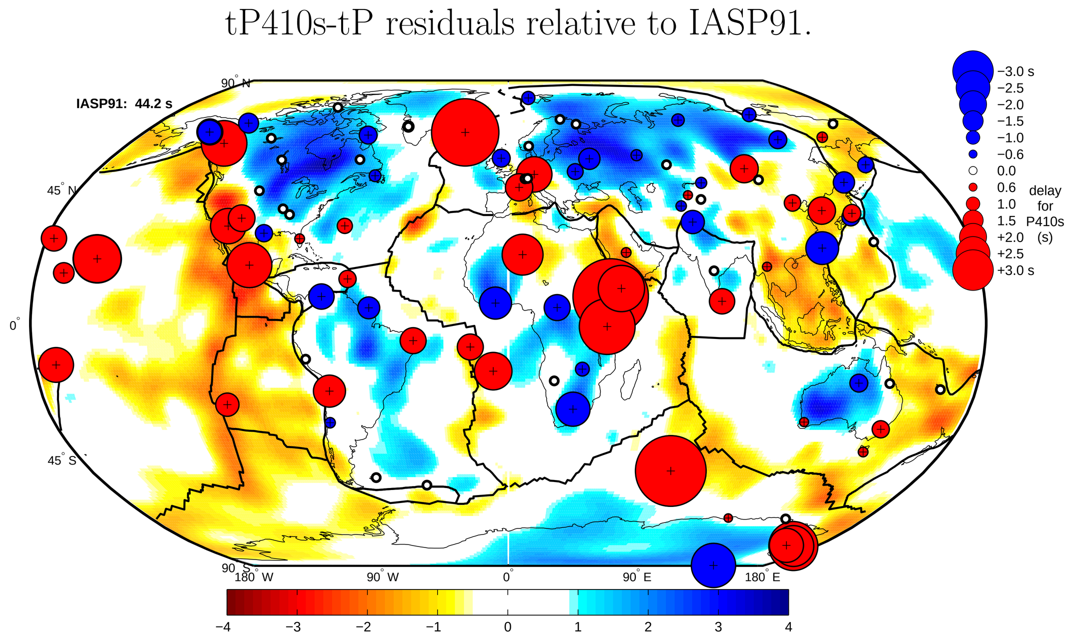

Figure 5. Travel times for conversions at the MTZ discontinuities are strongly affected by 3-D velocity heterogeneities in the crust and shallow upper mantle. To qualitatively represent the confidence in our measurements, we superimposed our residuals $(tP410s\text{-}tP)_{obs}\text{-}(tP410s\text{-}tP)_{IASP91}$ on the Sv velocity model of [3] in which we radially averaged anomalies between 40 and 410 km depth. Positive residuals (late arrivals) are shown with plain red circles. Negative residuals (early arrivals) are shown with plain blue circles. In the tomographic model, fast and slow anomalies are in blue and red respectively. The IASP91 time reference value for P410s is 44.2 s after the direct P arrival. tP410s-tP residues strongly correlate with structures over the MTZ.

Observed MTZ differential travel times tP660s-tP410s.

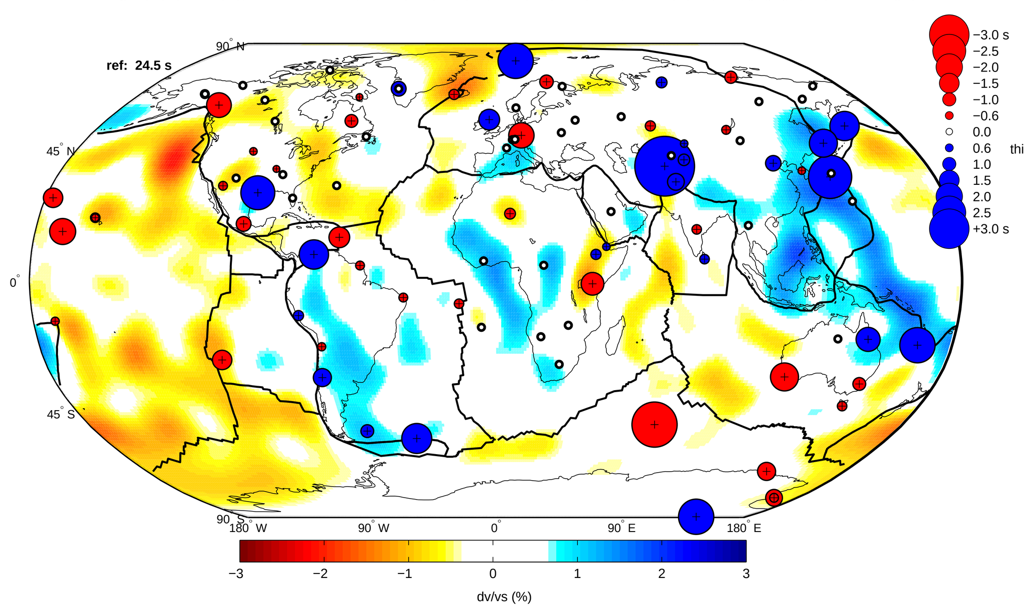

Figure 6. Differential travel times tP660s-tP410s depend on the thickness and pattern of seismic heterogeneities within the MTZ. Differential travel times under each station are represented relative to the global average MTZ thickness of 24.5 s. The IASP91 reference value for tP660s-tP410s is slightly weaker (24s). Positive (suggesting a thicker MTZ) and negative (suggesting a thinner MTZ) differential travel times are shown with plain blue (red) circles. The background velocity model used here is a radial average of S20RTS ([4]) through the transition zone. Fast (slow) anomalies are in blue (red). Our travel-time measurements are in qualitative agreement with S20RTS despite the different lateral resolution of both data sets (few hundred of km for Pds waves and about 2000 km in S20RTS).

Statistics on measurements.

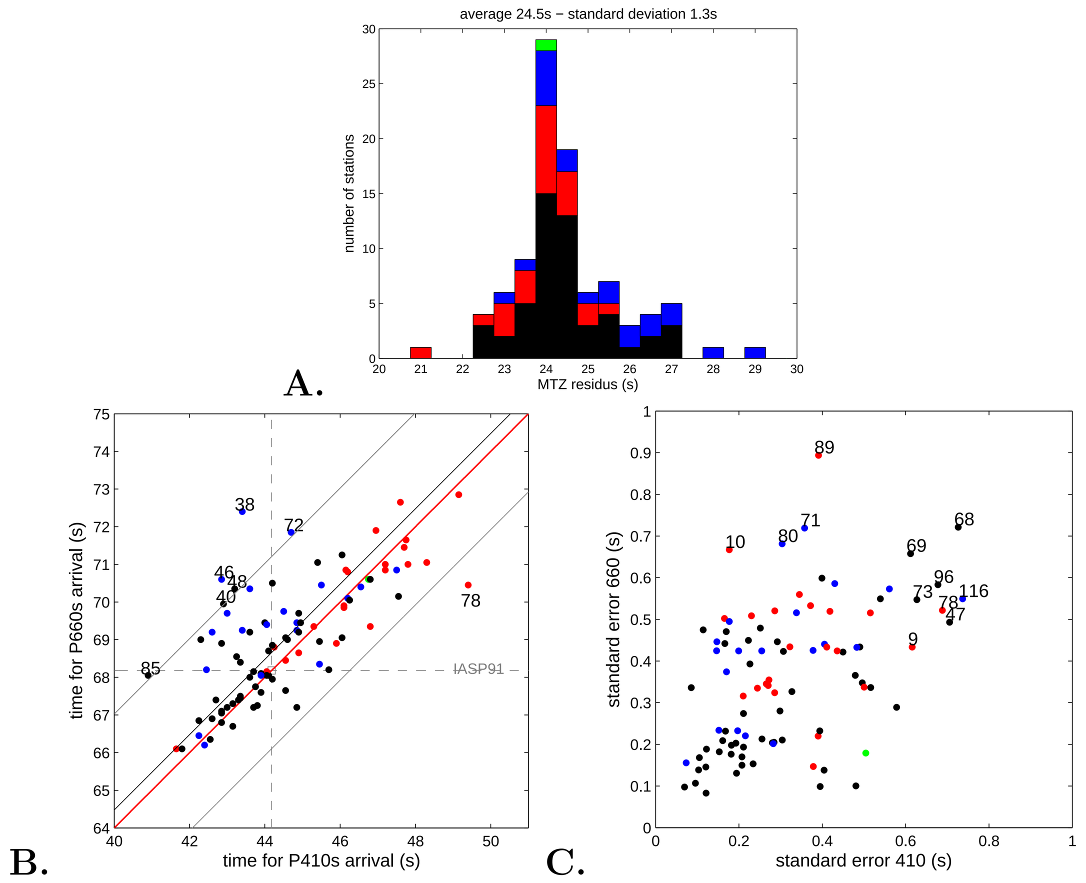

Figure 7 The red, blue and black colors identify the measurements for "subduction zones", "plume stations" and "normal mantle", the green color being associated to the station belonging to both "plume" and "subduction" regions. **A.** Our measurements are distributed around the mean value of 24.5 s with a standard deviation of 1.3 s. **B.** : P660s relative to P410s arrival times. Red line is the IASP91 reference value of 24 s. Points over (under) this line represent thicker (thinner) MTZ measurements. Influence of the crust and upper mantle is clearly visible with slow (fast) mantle on the right (left) part. "Hotspot" measurements are associated with slow velocity anomalies in the mantle lying above the MTZ. "Subduction zone" measurements show more scatter than other regions. **C.** : Measurement errors estimated from a bootstrap resampling technique. "Normal mantle" gives more reliable results than other regions.

Plume Regions

Supposing that the plume conduit associated to well-known hotspots has a radius of about 200 km (Montelli et al. 2006) and that P-to-s conversions sample approximately a 300-km radius region at the 660 km discontinuity under the station, we built our "hotspot stations" subset with stations located at less than 600 km from the hotspot list given in [6] and [5]. After applying our selection criteria, we were able to measure the MTZ thickness at 23 stations on an initial subset of 28 stations. **The average MTZ thickness for "plume" stations is 24 s with a standard deviation of 0.7 s.** This average does not differ significantly from the "normal mantle" in spite of slightly higher standard errors than for "normal mantle" stations (figure 7.C.).

Both **table 2 and 3** present results obtained at each station.

hotspot	station	tP660s-tP410s (s)	standard error (s)
Afar, Ethiopie	FURI	25.3	0.5
Afar, Ethiopie	ATD	25.1	0.6
Ascencion	ASCN	23.8	0.6
Bermuda	BBSR	24.1	0.7
Crozet	CRZF	-	-
East Australia	TAU	23.7	0.7
Easter/Sala Y Gomez	RPN	23.0	0.9
Eiffel	SSB	24.6	0.4
Eiffel	BFO	24.5	0.3
Eiffel	ECH	24.1	0.6
Eiffel	GRFO	22.6	0.4
Fernando do Norona	RCBR	23.8	0.6
Guadalupe	PFO	-	-
Hawaii	KIP	23.8	0.5

table 2

hotspot	station	tP660s-tP410s (s)	standard error (s)
Hawaii	KIP	23.9	0.5
Hoggar Mountains, ALGER	TAM	23.7	0.7
Iceland	BORG	23.7	0.5
Kerguelen	PAF	-	-
Lac Victoria	KMBO	22.8	0.6
Mount Erebus	SBA	23.8	0.6
Mount Erebus	SBA	23.2	0.5
Mount Erebus	VNDA	-	-
New England	BOSA	24.5	0.4
Raton, New Mexico (GVP)	ANMO	24.7	0.4
Samoa	AFI	23.9	0.5
ST. Helena	SHEL	25.0	0.4
Vema Seamount	SUR	-	-
Yellowstone	RSSD	23.9	0.7

table 3

Subduction Zones

We use the slab contours of the RUM model ([7]) to associate with "slabs" all the stations located at less than 600 km from a contour. Our analysis assumes 1-D stratification of the upper mantle and is not well suited to study complex structures in slab regions. For this reason, some of our measurements are built by stacking over a selected range of back-azimuth. The choice of back-azimuth is conditioned by : 1. the data quality and 2. no evidence for complex structures interfering with observations of conversions at the MTZ discontinuities. Figure 7.A. and B. show an example of such complexity.

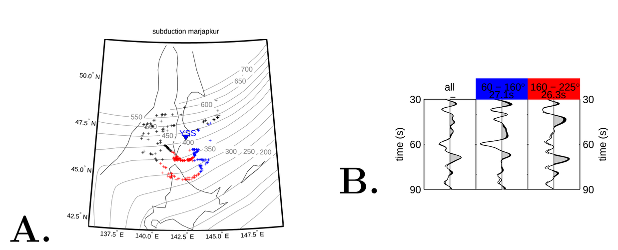

Figure 7. A. Example of back-azimuth selection on north-west pacific station YSS. Slab contours are from the RUM model. **B.** A strong negative amplitude interferes on back-azimuth 60 to 160°.

subduction	station	tP660s-tP410s (s)	standard error (s)
tonga	AFI	23.9	0.5
aleutians	ADK	-	-
aleutians	COL	24.2	0.3
aleutians	COLA	23.8	0.4
aleutians	KDAK	-	-
aleutians	PET	26.7	0.3
assam	CHTO	24.6	0.5
camerica	UNM	-	-
caribbean	FDF	-	-

table 4

subduction	station	tP660s-tP410s (s)	standard error (s)
hellas	ANTO	-	-
hindu1	GAR	29.0	0.7
hindu1	NIL	25.8	0.5
hindu2	AAK	24.4	0.3
hindu2	WUS	25.4	0.2
marjapkur	INCN	23.9	0.4
marjapkur	INU	27.8	0.4
marjapkur	MAJO	25.0	0.5
marjapkur	OGS	24.2	0.6

table 5

subduction	station	tP660s-tP410s (s)	standard error (s)
marjapkur	TSK	-	-
marjapkur	YSS	26.6	0.4
ryukyus	TATO	-	-
samerica	LVC	23.9	0.6
samerica	NNA	25.3	0.8
samerica	PEL	25.9	0.5
ssandwich	HOPE	26.8	0.8
vanuatu	NOUC	27.2	0.8

table 6

Among an initial subset of 26 stations, we obtain 19 MTZ thickness measurements. **The subset average (25.5 s) is largely thicker than the global average (24.5 s)** and we observe 1.5 s deviation standard around it.

Normal Mantle

Our "Normal mantle" dataset is composed of the 72 remaining stations. 50 of them give measurements for the MTZ thickness. **We find an average of 24.5s** with a 1.1s standard deviation.

One "normal mantle" station shows abnormal thickening of the MTZ : station HKT in north-America with 27.2 ± 0.5 s (station 40 in figure 4). A possible explanation for the anomalous MTZ thickness at station HKT might be the presence in the MTZ of a fragment of the subducted Farallon plate, as imaged by [8] (figure 8).

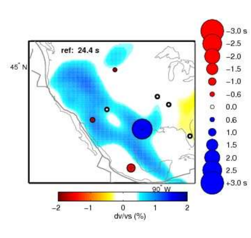

Figure 8. Our tP660s-tP410s differential travel times are superimposed on a radial average through the MTZ of the regional shear-wave velocity model for north America NA04 ([8]).

Discontinuity Detection

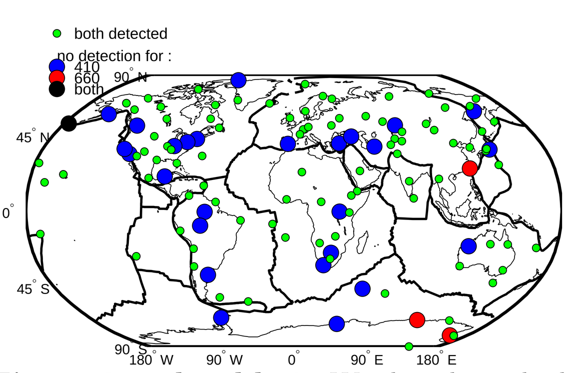

no 410				no 660	both undetectable
ABKT	KURK	PAF	SUR	CASY	ADK
ALE	LBTB	PFO	SYO	TATO	MPG
ANTO	LLLB	PMSA	TEIG	UNM	
CRZF	MA2	PTGA	TRQA	VNDA	
HRV	MBAR	SAML	TSK		
KDAK	MBWA	SCZ	WCI		
KIV	PAB	SSPA			

Figure 8 and Table 7. We show here the location where one or two of the discontinuities are not detected in this study, despite a set of high quality data.

References

[1] Ligorrìa, J. and Ammon,Iterative deconvolution and receiver function estimation C., Bull. Seismol. Am.,vol 85, 1395-1400, 1999.

[2] Kennett, B.L.N., Iaspei 1991 seismological tables, Res. Sch. of Earth Sci. Int., Aust. Nat. Univ., Canberra, 1991.

[3] Debayle, E., Kennett, B.L.N., Priestley K., Global azimuthal seismic anisotropy and the unique plate-motion deformation of Australia, Nature 433, 509-512 (2005).

[4] Ritsema, J. and van Heijst, H. J., Seismic imaging of structural heterogeneity in Earth's mantle: Evidence for large-scale mantle flow, Science Progress, 83, 243-259, 2000.

[5] Courtillot, V., Davaille, A., Besse, J. Stock, J. 2003, Three distinct types of hotspots in the Earths mantle, Earth and Planetary Science Letters 205 3-4, 295-308.

[6] Montelli, R., G. Nolet, F. A. Dahlen, and G. Masters (2006), A catalogue of deep mantle plumes: New results from finite-frequency tomography, Geochem. Geophys. Geosyst., 7, Q11007, doi:10.1029/2006GC001248.

[7] Gudmundsson, ., and M. Sambridge (1998), A regionalized upper mantle (RUM) seismic model, J. Geophys. Res., 103(B4), 71217136.

[8] Van der Lee, S., and A. Frederiksen, 2005, Surface Wave Tomography applied to the North American upper mantle, in AGU Monograph "Seismic Data Analysis and Imaging With Global and Local Arrays", Eds: Nolet and Levander, 67-80.